Passive control of a periodic structure using a network of periodically-coupled piezoelectric shunt circuits

Ghislain Raze, Jennifer Dietrich, Ahmad Paknejad, Boris Lossouarn, Guoying Zhao, Arnaud Deraemaeker, Christophe Collette, Gaëtan Kerschen

Passive control of a periodic structure using a network of periodically-coupled piezoelectric shunt circuits

G. Raze [1], **J. Dietrich** [1], **A. Paknejad** [2], **B. Lossouarn** [3], **G. Zhao** [2], **A. Deraemaeker** [4], **C. Collette** [1,2], **G. Kerschen** [1]

[1] Aerospace and Mechanical Engineering Department, University of Liège,
Allée de la Découverte 9, 4000 Liège, Belgium

[2] Department of Bio-, Electro- and Mechanical Systems, Université Libre de Bruxelles,
Av. F.D Roosevelt 50, 1050 Brussels, Belgium

[3] Laboratoire de Mécanique des Structures et des Systèmes Couplés, Conservatoire national des arts et métiers, 292 Rue Saint-Martin, 75003 Paris, France

[4] Building Architecture and Town Planning (BATir) Department, Université Libre de Bruxelles,
Av. F.D Roosevelt 50, 1050 Brussels, Belgium

Abstract

This work proposes a method to synthesize an electrical network which, when coupled to a complex periodic or nearly-periodic structure through an array of piezoelectric transducers, provides multimodal vibration mitigation. The structure is decomposed into multiple substructures and a reduced-order model is built for each of them. From these models, it is possible to synthesize a network with simple algebraic transformations. The link between these transformations and electromechanical modal coupling is derived, and conditions are given in order to guarantee the passivity of the electrical network. The proposed approach is illustrated on a bladed rail, for which damping of one or multiple families of blade modes is demonstrated.

1 Introduction

In mechanical and aerospace engineering, periodic structures such as truss beam structures, wheels and bladed disks are a frequent encounter. These structures tend to be light, mainly for performance requirements. An undesirable consequence of such characteristic is that they are becoming flexible. There is also a growth in the use of monolithic structures, but they often exhibit low structural damping. These issues combined with mistuning can drastically reduce their lifespan because of high cycle fatigue. Enhanced damping processes for such structures constitute an active field of research.

Among the existing solutions, there has been a growing interest for piezoelectric shunt damping [1], whereby a piezoelectric transducer bonded to a vibrating structure converts part of its mechanical energy to electrical energy, which is then dissipated in resistive elements, resulting in effective structural damping. Mokrani and Preumont [2] investigated the performance of this approach applied to integrally bladed disks. Another solution involving piezoelectric coupling is to use electrical networks interconnecting multiple piezoelectric transducers, which generally allows to control multiple modes. Alessandroni et al [3] showed that effective vibration mitigation can be achieved provided these networks mimic the modal characteristics of the structure. The efficiency of this kind of approach was experimentally demonstrated on structures such as plates [4, 5]. It was also applied to a bladed disk using an equivalent spring-mass model [6], and was shown to still be relatively effective in presence of mistuning or non-engine order excitation [7]. Because of the simplifications made, this model is able to reproduce qualitatively but not quantitatively the dynamics of real bladed disks. In this respect, a technique based on standard modeling techniques such as the finite element

method [8, 9] seems more attractive. Giorgio et al [10] proposed a general method to design an electrical network connected to several piezoelectric transducers. Shortcomings of that method are that to damp n modes this method requires n piezoelectric transducers, and it is also needed to solve a quadratic system of n^2 equations.

This work aims to derive a method to design a network based on a finite element model of a periodic (or nearly-periodic) structure. Taking advantage of its nature, a reduced-order model (ROM) of the structure is built from an assembly of ROMs of its substructures. These ROMs allow to synthesize subnetworks with a few electrical degrees of freedom, which, when assembled, provide multimodal damping on the overall structure. Section 2 briefly provides reminders on the salient features of resonant piezoelectric shunt damping. In Section 3, a ROM of a structure is built from an assembly of ROMs of substructures. Section 4 then shows how the ROM can be used to synthesize an electrical subnetwork analogous to the mechanical substructure. Upon assembling the mechanical substructures and electrical subnetworks to form the whole electromechanical system, multimodal damping of the structure is achieved. This performance is illustrated with a bladed rail in Section 5. The conclusions of this work are eventually drawn in Section 6.

2 Theoretical reminders: parallel RL shunt

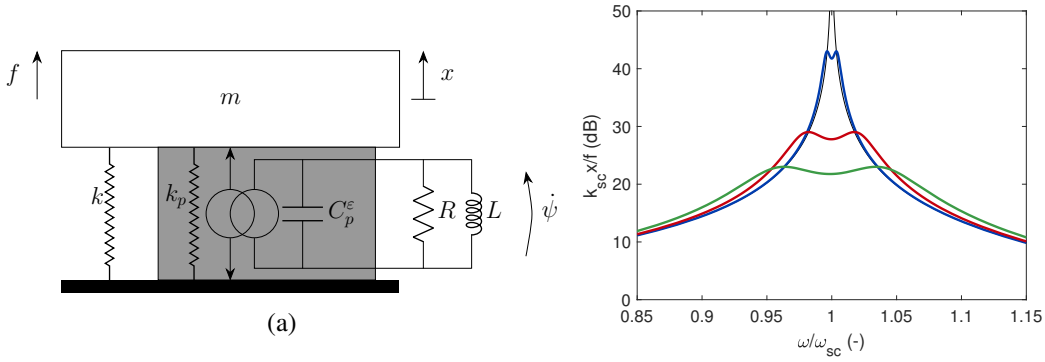

(a) (b)

Figure 1: Schematic representation of the electromechanical system (a) and FRF of the structure (b) with short-circuited patches (—) and with a parallel RL shunt circuit (—: $K_c = 0.01$, —: $K_c = 0.05$, —: $K_c = 0.1$).

Figure 1(a) depicts a single-degree-of-freedom oscillator to which is bonded a piezoelectric transducer connected to a parallel RL shunt circuit. The structure is excited by an external forcing f and responds with a displacement x. The direct piezoelectric effect also creates a flux linkage $\psi = \int V dt$ (where V is the voltage across the electrodes of the transducer). The electromechanical equations of the system read

$$\begin{cases} m\ddot{x} + c\dot{x} + k_{sc}x + \gamma\dot{\psi} & = f \\ C_p^\varepsilon\ddot{\psi} + \dfrac{1}{R}\dot{\psi} + \dfrac{1}{L}\psi - \gamma\dot{x} & = 0 \end{cases}, \tag{1}$$

where m is the structural mass, $k_{sc} = k + k_p$ is the structural stiffness with short-circuited transducer, γ is a coupling constant, C_p^ε is the capacitance at constant strain, and R and L are the resistance and inductance of the shunt circuit, respectively [10, 11]. From the parameters appearing in Equation (1), it is possible to define a short-circuit resonance frequency ω_{sc} and a dimensionless quantity called the effective electromechanical coupling factor (EEMCF) [9] K_c as

$$\omega_{sc}^2 = \frac{k_{sc}}{m}, \qquad K_c^2 = \frac{\gamma^2}{C_p^\varepsilon k_{sc}}. \tag{2}$$

The EEMCF assesses the coupling between the mechanical and electrical dynamics. Knowing C_p^ε, ω_{sc}

and K_c, the resistance and inductance of the shunt circuit may be tuned in order to reduce the maximum amplitude of vibration of the mechanical oscillator under harmonic excitation. For instance, using the tuning rules from Yamada et al [11],

$$L = \frac{2}{(2 - K_c^2)\omega_{sc}^2 C_p^\varepsilon}, \qquad R = \sqrt{\frac{2}{3K_c^2}} \frac{1}{\omega_{sc} C_p^\varepsilon}. \tag{3}$$

Note that in general $K_c \ll 1$, so that $LC_p^\varepsilon \approx \omega_{sc}^{-2}$, i.e., the electrical resonance frequency is equal to the short-circuit mechanical one. The amplitude of the frequency response function (FRF) of the structure with this shunt circuit is shown in Figure 1(b) for various values of the EEMCF. Clearly, the stronger the coupling, the better the performance in terms of vibration attenuation.

If multiple resonance frequencies are to be damped, the problem becomes more involved. Section 4 will discuss one way to achieve this and will base itself on results presented in the present section as well as results of the next section.

3 Reduced-order model

This work deals with structures which can be seen as an assembly of substructures, a category in which periodic structures fall. A schematic representation of this situation is shown in Figure 2. It is considered that each substructure may be connected to its neighboring peers through its left and right interfaces for simplicity of the derivation, but the results can easily be generalized to more complex interfaces.

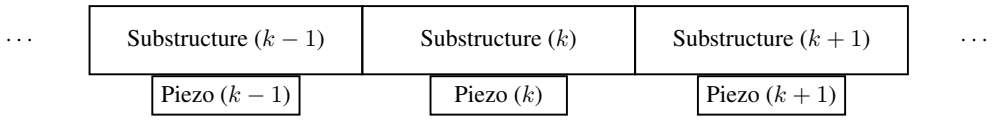

Figure 2: Schematics of the piezoelectric structure.

The model of the structure may possess a large number of degrees of freedom (DOFs). ROMs are typically used to reduce this number, while retaining an accurate description of the structure's dynamics. Model-order reduction can also be applied to each substructure. Adopting such approach will allow to design an electrical network as an assembly of subnetworks built from the ROMs of substructures, as shall be shown in the next section. The goal of this section is thus to give a procedure to build ROMs of substructures with a very few number of DOFs.

3.1 Craig-Bampton reduction procedure for piezoelectric structures

A structure or substructure with bonded piezoelectric transducers is considered. The vector of generalized mechanical DOFs $\mathbf{x}$ is partitioned into boundary and internal DOFs indicated by subscripts B and I, respectively. The governing equations of this structure can be obtained through finite element modeling [8, 9]. They read

$$\begin{bmatrix} \mathbf{M}_{BB} & \mathbf{M}_{BI} & \mathbf{0} \\ \mathbf{M}_{IB} & \mathbf{M}_{II} & \mathbf{0} \\ \mathbf{0} & \mathbf{0} & \mathbf{0} \end{bmatrix} \begin{bmatrix} \ddot{\mathbf{x}}_B \\ \ddot{\mathbf{x}}_I \\ \ddot{\mathbf{V}} \end{bmatrix} + \begin{bmatrix} \mathbf{K}_{BB} & \mathbf{K}_{BI} & \boldsymbol{\Gamma}_B \\ \mathbf{K}_{IB} & \mathbf{K}_{II} & \boldsymbol{\Gamma}_I \\ \boldsymbol{\Gamma}_B^T & \boldsymbol{\Gamma}_I^T & -\mathbf{K}_e \end{bmatrix} \begin{bmatrix} \mathbf{x}_B \\ \mathbf{x}_I \\ \mathbf{V} \end{bmatrix} = \begin{bmatrix} \mathbf{f}_B \\ \mathbf{f}_I \\ -\mathbf{q} \end{bmatrix}, \tag{4}$$

where $\mathbf{M}$ and $\mathbf{K}$ denote structural mass and stiffness matrices, respectively, $\boldsymbol{\Gamma}$ is a piezoelectric coupling matrix, $\mathbf{K}_e$ is a capacitance matrix, $\mathbf{f}$ is a vector of generalized mechanical loads and $\mathbf{V}$ and $\mathbf{q}$ are vectors of voltages and charges associated with the electrodes of the piezoelectric transducers, respectively. Following the classical Craig-Bampton reduction procedure [12, 13], the boundary and electrical DOFs are retained, while the internal DOFs are assumed unforced ($\mathbf{f}_I = 0$) and are approximated by

$$\mathbf{x}_I \approx \boldsymbol{\Phi}_c \mathbf{x}_B + \boldsymbol{\Phi}_e \mathbf{V} + \boldsymbol{\Phi}_I \boldsymbol{\eta}_I, \tag{5}$$

where the constraint modes are given by

$$\boldsymbol{\Phi}_c = -\mathbf{K}_{II}^{-1}\mathbf{K}_{IB}, \tag{6}$$

the piezoelectric constraint modes are given by

$$\boldsymbol{\Phi}_e = -\mathbf{K}_{II}^{-1}\boldsymbol{\Gamma}_I, \tag{7}$$

and the retained mass-normalized component normal modes (CNM) are defined by

$$\mathbf{K}_{II}\boldsymbol{\Phi}_I = \mathbf{M}_{II}\boldsymbol{\Phi}_I\boldsymbol{\Omega}_I^2, \qquad \boldsymbol{\Phi}_I^T\mathbf{M}_{II}\boldsymbol{\Phi}_I = \mathbf{I}, \qquad \boldsymbol{\Phi}_I^T\mathbf{K}_{II}\boldsymbol{\Phi}_I = \boldsymbol{\Omega}_I^2, \tag{8}$$

where $\mathbf{I}$ is the identity matrix, $\boldsymbol{\Omega}_I$ is a diagonal matrix containing the CNM angular frequencies, $\boldsymbol{\eta}_I$ is the vector of associated modal coordinates and superscript T denotes matrix transposition. Equation (5) defines a reduction matrix as

$$\begin{bmatrix} \mathbf{x}_B \\ \mathbf{x}_I \\ \mathbf{V} \end{bmatrix} = \begin{bmatrix} \mathbf{I} & \mathbf{0} & \mathbf{0} \\ \boldsymbol{\Phi}_c & \boldsymbol{\Phi}_I & \boldsymbol{\Phi}_e \\ \mathbf{0} & \mathbf{0} & \mathbf{I} \end{bmatrix} \begin{bmatrix} \mathbf{x}_B \\ \boldsymbol{\eta}_I \\ \mathbf{V} \end{bmatrix} = \mathbf{R}_{CB} \begin{bmatrix} \mathbf{x}_B \\ \boldsymbol{\eta}_I \\ \mathbf{V} \end{bmatrix}. \tag{9}$$

The reduced mass and stiffness matrices are obtained as

$$\mathbf{M}_{CB} = \mathbf{R}_{CB}^T\mathbf{M}\mathbf{R}_{CB} = \begin{bmatrix} \widetilde{\mathbf{M}}_{BB} & \widetilde{\mathbf{M}}_{BI} & \widetilde{\mathbf{M}}_{BE} \\ \widetilde{\mathbf{M}}_{IB} & \mathbf{I} & \widetilde{\mathbf{M}}_{IE} \\ \widetilde{\mathbf{M}}_{EB} & \widetilde{\mathbf{M}}_{EI} & \widetilde{\mathbf{M}}_{EE} \end{bmatrix} \tag{10}$$

and

$$\mathbf{K}_{CB} = \mathbf{R}_{CB}^T\mathbf{K}\mathbf{R}_{CB} = \begin{bmatrix} \widetilde{\mathbf{K}}_{BB} & \mathbf{0} & \widetilde{\mathbf{K}}_{BE} \\ \mathbf{0} & \boldsymbol{\Omega}_I^2 & \mathbf{0} \\ \widetilde{\mathbf{K}}_{EB} & \mathbf{0} & \widetilde{\mathbf{K}}_{EE} \end{bmatrix}, \tag{11}$$

respectively, where $\mathbf{M}$ and $\mathbf{K}$ are the full mass and stiffness matrices featured in Equation (4). The expressions of the submatrices are not given here for conciseness. Equation (10) indicates that piezoelectric coupling is no longer represented with static coupling terms (as in Equation (4)), but also features non-trivial inertial coupling terms in the reduced model. To retrieve a static coupling, the following transformation matrix that modifies the CNM coordinates $\boldsymbol{\eta}_I$ to $\boldsymbol{\upsilon}_I$ is introduced

$$\mathbf{R}_{MCB} = \begin{bmatrix} \mathbf{I} & \mathbf{0} & \mathbf{0} \\ \mathbf{0} & \mathbf{I} & -\widetilde{\mathbf{M}}_{IE} \\ \mathbf{0} & \mathbf{0} & \mathbf{I} \end{bmatrix}, \qquad \begin{bmatrix} \mathbf{x}_B \\ \boldsymbol{\eta}_I \\ \mathbf{V} \end{bmatrix} = \mathbf{R}_{MCB} \begin{bmatrix} \mathbf{x}_B \\ \boldsymbol{\upsilon}_I \\ \mathbf{V} \end{bmatrix} \tag{12}$$

and the modified Craig-Bampton (MCB) reduced mass and stiffness matrices are obtained as

$$\mathbf{M}_{MCB} = \mathbf{R}_{MCB}^T\mathbf{M}_{CB}\mathbf{R}_{MCB}, \qquad \mathbf{K}_{MCB} = \mathbf{R}_{MCB}^T\mathbf{K}_{CB}\mathbf{R}_{MCB}. \tag{13}$$

It can be shown that these matrices contain the following entries

$$\mathbf{M}_{MCB} = \begin{bmatrix} \widetilde{\mathbf{M}}_{BB} & \widetilde{\mathbf{M}}_{BI} & \left(\boldsymbol{\Phi}_c^T\mathbf{M}_{II} - \mathbf{M}_{BI}\right)\left(\mathbf{M}_{II}^{-1} - \boldsymbol{\Phi}_I\boldsymbol{\Phi}_I^T\right)\mathbf{M}_{II}\boldsymbol{\Phi}_e \\ \widetilde{\mathbf{M}}_{IB} & \mathbf{I} & \mathbf{0} \\ \boldsymbol{\Phi}_e^T\mathbf{M}_{II}\left(\mathbf{M}_{II}^{-1} - \boldsymbol{\Phi}_I\boldsymbol{\Phi}_I^T\right)\left(\mathbf{M}_{II}\boldsymbol{\Phi}_c - \mathbf{M}_{IB}\right) & \mathbf{0} & \boldsymbol{\Phi}_e^T\mathbf{M}_{II}\left(\mathbf{M}_{II}^{-1} - \boldsymbol{\Phi}_I\boldsymbol{\Phi}_I^T\right)\mathbf{M}_{II}\boldsymbol{\Phi}_e \end{bmatrix} \tag{14}$$

and

$$\mathbf{K}_{MCB} = \begin{bmatrix} \widetilde{\mathbf{K}}_{BB} & \mathbf{0} & \boldsymbol{\Gamma}_B + \boldsymbol{\Phi}_c^T \boldsymbol{\Gamma}_I \\ \mathbf{0} & \boldsymbol{\Omega}_I^2 & \boldsymbol{\Phi}_I^T \boldsymbol{\Gamma}_I \\ \boldsymbol{\Gamma}_B^T + \boldsymbol{\Gamma}_I^T \boldsymbol{\Phi}_c & \boldsymbol{\Gamma}_I^T \boldsymbol{\Phi}_I & -\mathbf{K}_e - \boldsymbol{\Gamma}_I^T \left(\mathbf{K}_{II}^{-1} - \boldsymbol{\Phi}_I \boldsymbol{\Omega}_I^{-2} \boldsymbol{\Phi}_I^T \right) \boldsymbol{\Gamma}_I \end{bmatrix}. \tag{15}$$

Upon performing the transformation given by Equation (13), part of the inertial coupling terms have been transformed back to static coupling terms. As shown by the mass matrix in Equation (14), there remains non-zero entries associated with the electrical DOFs. To remove these terms, the following assumption is made

$$\mathbf{M}_{II}^{-1} - \boldsymbol{\Phi}_I \boldsymbol{\Phi}_I^T \approx 0. \tag{16}$$

It can be recognized (Equation (8)) that this equation consists in the mass matrix associated to the internal DOFs minus its spectral expansion trucated to the set of retained CNMs [13], which justifies the approximation in the framework of a ROM. Thus, the approximation is made on the reduced mass matrix:

$$\mathbf{M}_{MCB} \approx \begin{bmatrix} \widetilde{\mathbf{M}}_{BB} & \widetilde{\mathbf{M}}_{BI} & \mathbf{0} \\ \widetilde{\mathbf{M}}_{IB} & \mathbf{I} & \mathbf{0} \\ \mathbf{0} & \mathbf{0} & \mathbf{0} \end{bmatrix} \tag{17}$$

so that no generalized inertia load acts on the electric DOFs, as in Equation (4).

3.2 Characteristic constraint modes

In this subsection, the different substructures are discriminated by indexing their associated terms with bracketed superscripts. To accurately describe the dynamics of the substructures' boundaries, each DOF in these boundaries should be retained. This may lead to a large number of DOFs in the reduced model, especially if the interfaces are complex. Since the goal of this section is to provide a ROM with as few DOFs as possible, a reduction of the interface DOFs is sought. The characteristic constraint modes (CCMs) of the interfaces can be used as reduction bases to simplify the description of these interfaces [14]. The boundary DOFs B are now splitted into DOFs belonging to the left (L) and right (R) interface. The stiffness matrix of the full structure can be obtained by assembling the stiffness matrices of all the substructures. Focusing on the interface between substructure k and $k+1$, this matrix reads

$$\mathbf{K}_{Str} = \begin{bmatrix} \ddots & \ddots & & & \\ \ddots & \mathbf{K}_{II}^{(k)} & \mathbf{K}_{IR}^{(k)} & \mathbf{0} & \\ & \mathbf{K}_{RI}^{(k)} & \mathbf{K}_{RR}^{(k)} + \mathbf{K}_{LL}^{(k+1)} & \mathbf{K}_{LI}^{(k+1)} & \\ & \mathbf{0} & \mathbf{K}_{LI}^{(k+1)} & \mathbf{K}_{II}^{(k+1)} & \ddots \\ & & & \ddots & \ddots \end{bmatrix} \tag{18}$$

and the mass matrix of the full structure features a similar form. The CCMs are obtained by performing the following modal analysis

$$\left(\mathbf{K}_{RR}^{(k)} + \mathbf{K}_{LL}^{(k+1)} \right) \boldsymbol{\Psi}_{CCM}^{(k)} = \left(\mathbf{M}_{RR}^{(k)} + \mathbf{M}_{LL}^{(k+1)} \right) \boldsymbol{\Psi}_{CCM}^{(k)} \boldsymbol{\Omega}_{CCM}^2. \tag{19}$$

Using a reduced subset of CCMs, the generalized DOFs at the interface may then be approximated by

$$\mathbf{x}_R^{(k)} = \mathbf{x}_L^{(k+1)} \approx \boldsymbol{\Psi}_{CCM}^{(k)} \boldsymbol{\mu}_R^{(k)} = \boldsymbol{\Psi}_{CCM}^{(k)} \boldsymbol{\mu}_L^{(k+1)}, \tag{20}$$

where $\boldsymbol{\mu}^{(k)}$ is the vector of modal coordinates of the CCMs. This relation can be used to define a reduction matrix for each substructure

$$\begin{bmatrix} \mathbf{x}_L^{(k)} \\ \mathbf{x}_R^{(k)} \\ \boldsymbol{\upsilon}_I^{(k)} \\ \mathbf{V}^{(k)} \end{bmatrix} = \begin{bmatrix} \boldsymbol{\Psi}_{CCM}^{(k-1)} & \mathbf{0} & \mathbf{0} & \mathbf{0} \\ \mathbf{0} & \boldsymbol{\Psi}_{CCM}^{(k)} & \mathbf{0} & \mathbf{0} \\ \mathbf{0} & \mathbf{0} & \mathbf{I} & \mathbf{0} \\ \mathbf{0} & \mathbf{0} & \mathbf{0} & \mathbf{I} \end{bmatrix} \begin{bmatrix} \boldsymbol{\mu}_L^{(k)} \\ \boldsymbol{\mu}_R^{(k)} \\ \boldsymbol{\upsilon}_I^{(k)} \\ \mathbf{V}^{(k)} \end{bmatrix} = \mathbf{R}_{CCM}^{(k)} \begin{bmatrix} \boldsymbol{\mu}_L^{(k)} \\ \boldsymbol{\mu}_R^{(k)} \\ \boldsymbol{\upsilon}_I^{(k)} \\ \mathbf{V}^{(k)} \end{bmatrix} \tag{21}$$

and to obtain the reduced mass and stiffness matrices of each substructure, respectively, as

$$\mathbf{M}_{MCB-CCM}^{(k)} = \left(\mathbf{R}_{CCM}^{(k)}\right)^T \mathbf{M}_{MCB}^{(k)} \mathbf{R}_{CCM}^{(k)} = \begin{bmatrix} \widehat{\mathbf{M}}^{(k)} & \mathbf{0} \\ \mathbf{0} & \mathbf{0} \end{bmatrix} \tag{22}$$

and

$$\mathbf{K}_{MCB-CCM}^{(k)} = \left(\mathbf{R}_{CCM}^{(k)}\right)^T \mathbf{K}_{MCB}^{(k)} \mathbf{R}_{CCM}^{(k)} = \begin{bmatrix} \widehat{\mathbf{K}}^{(k)} & \widehat{\boldsymbol{\Gamma}}^{(k)} \\ \left(\widehat{\boldsymbol{\Gamma}}^{(k)}\right)^T & -\widehat{\mathbf{K}}_e^{(k)} \end{bmatrix}. \tag{23}$$

In the sequel, superscript (k) shall be dropped, being understood that one is working with a specific substructure at a time. The left and right reduced interface DOFs shall also be gathered into boundary interface DOFs for brevity, i.e., $B^T = [L^T, R^T]$.

4 Electrical network

Vibration mitigation of a piezoelectric structure may be achieved by piezoelectric coupling with an electrical network if the latter possesses identical modal characteristics to those of the former [3]. The goal of this section is thus to design such network. It is considered in this work that each substructure has a single transducer. Starting from the ROM of a substructure, a subnetwork is designed, which has the same resonant frequencies and possess interface nodes which are analogous to the interfaces of its mechanical counterpart. Since this ROM has been obtained from a Craig-Bampton reduction, the resonance frequencies of the (full model of the) substructure and those of the subnetwork are identical when their interface DOFs are fixed. The subnetwork also integrates the piezoelectric transducer in order to couple it with the substructure. Assembling the substructure and the subnetworks as depicted in Figure 3, an overall electromechanical system is formed in which vibration mitigation of targeted modes is achieved.

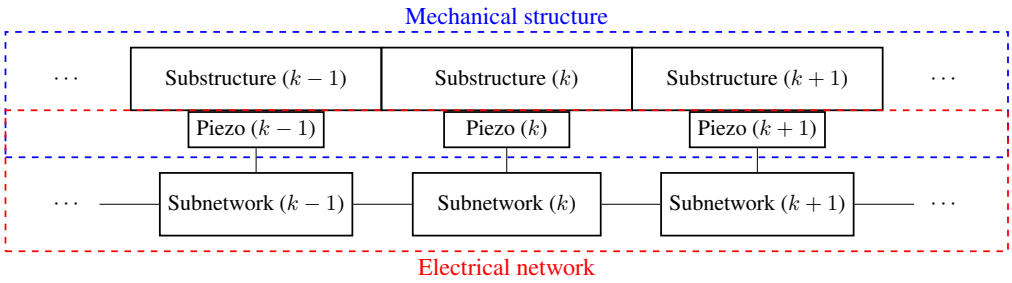

Figure 3: Schematics of the electromechanical system.

4.1 Governing equations

A subsystem composed of an undamped substructure coupled to an electrical subnetwork is governed by the equations

$$\begin{cases} \widehat{\mathbf{M}}\ddot{\mathbf{x}} + \widehat{\mathbf{K}}\mathbf{x} + \boldsymbol{\Gamma}_{EM}\dot{\boldsymbol{\psi}} & = \mathbf{f} \\ \mathbf{C}\ddot{\boldsymbol{\psi}} + \mathbf{S}\dot{\boldsymbol{\psi}} + \mathbf{B}\boldsymbol{\psi} - \boldsymbol{\Gamma}_{EM}^T\dot{\mathbf{x}} & = \mathbf{0} \end{cases}, \tag{24}$$

where $\mathbf{x}$ is the ROM's vector of generalized mechanical degrees of freedom, $\mathbf{f}$ is the generalized load vector, $\boldsymbol{\psi}$ is the flux linkage vector (whose time derivative gives the nodal voltages), $\mathbf{C}$, $\mathbf{S}$ and $\mathbf{B}$ are electrical capacitance, conductance (inverse of resistance) and reluctance (inverse of inductance) matrices, respectively, and $\boldsymbol{\Gamma}_{EM}$ is a piezoelectric coupling matrix.

The Laplace transform of the electrical equation in Equation (24) indicates that the electrical subnetwork's dynamics are governed by the nodal admittance matrix $\mathbf{Y}$

$$\mathbf{Y}(s)\boldsymbol{\psi} = \boldsymbol{\Gamma}_{EM}^T\mathbf{x}, \qquad \mathbf{Y}(s) = s\mathbf{C} + \mathbf{S} + \frac{1}{s}\mathbf{B}. \tag{25}$$

The matrices $\mathbf{C}$ and $\mathbf{B}$ will be built from the ROM using the indirect electromechanical analogy [15], whereas $\mathbf{S}$ will be chosen to ensure optimal electrical damping.

4.2 Piezoelectric lumping transformation

It is now sought to derive an expression for the capacitance and reluctance matrices of a subnetwork from the mechanical mass and stiffness matrices of its associated substructure with short-circuited patch. The subnetwork is chosen to have the same number of DOFs as that of the ROM of the substructure. When assembled into the network, the subnetwork should behave analogously to the substructure within the structure, thereby securing a spatial similarity between the structure and the network. A simple way to ensure that is to use interface electrical DOFs $\boldsymbol{\psi}_B$ which are analogous to interface DOFs $\boldsymbol{\mu}_B$. The remaining electrical DOFs still need to be specified.

In order to couple the substructure and the subnetwork, the electrodes of the piezoelectric transducer hosted by the substructure must be connected to the subnetwork. One port of the electrical network is thus chosen as a host for this transducer. Now, the electrical DOFs $\boldsymbol{\psi}_B$ analogous to mechanical boundary DOFs must remain unaltered in order to ensure compatibility when assembling the subnetworks. Hence, one of the DOFs analogous to the CNMs is to be transformed to host the transducer. The analogous internal DOFs I are thus splitted into this piezoelectric DOF ($\boldsymbol{\psi}_P$) and remaining electrical DOFs analogous to the remaining CNMs ($\boldsymbol{\psi}_M$). A priori, $\boldsymbol{\psi}_P$ can be formed from any combination of the DOFs of the ROM. It is thus sought to find a network satisfying the following relation between the mechanical and electrical variables

$$\begin{bmatrix} \boldsymbol{\psi}_B \\ \boldsymbol{\psi}_M \\ \boldsymbol{\psi}_P \end{bmatrix} = \begin{bmatrix} \mathbf{D}_B\boldsymbol{\mu}_B \\ \mathbf{D}_M\boldsymbol{\upsilon}_M \\ \mathbf{W}^T\mathbf{x} \end{bmatrix} = \begin{bmatrix} \mathbf{D}_B & \mathbf{0} & \mathbf{0} \\ \mathbf{0} & \mathbf{D}_M & \mathbf{0} \\ \mathbf{W}_B^T & \mathbf{W}_M^T & \mathbf{W}_P^T \end{bmatrix} \begin{bmatrix} \boldsymbol{\mu}_B \\ \boldsymbol{\upsilon}_M \\ \boldsymbol{\upsilon}_P \end{bmatrix} = \mathbf{R}^{-1} \begin{bmatrix} \boldsymbol{\mu}_B \\ \boldsymbol{\upsilon}_M \\ \boldsymbol{\upsilon}_P \end{bmatrix}, \tag{26}$$

where $\mathbf{W}^T = [\mathbf{W}_B^T, \mathbf{W}_M^T, \mathbf{W}_P^T]$ is a vector describing how each electrical DOF is coupled to the piezoelectric transducer, and $\mathbf{D}_B$ and $\mathbf{D}_M$ are diagonal scaling matrices ensuring dimensional homogeneity. These quantities are arbitrary for now, and their influence shall be discussed in the next sections. The matrix $\mathbf{R}^{-1}$ can readily be inverted to yield the transformation matrix $\mathbf{R}$

$$\begin{bmatrix} \boldsymbol{\mu}_B \\ \boldsymbol{\upsilon}_M \\ \boldsymbol{\upsilon}_P \end{bmatrix} = \mathbf{R} \begin{bmatrix} \boldsymbol{\psi}_B \\ \boldsymbol{\psi}_M \\ \boldsymbol{\psi}_P \end{bmatrix}, \qquad \mathbf{R} = \begin{bmatrix} \mathbf{D}_B^{-1} & \mathbf{0} & \mathbf{0} \\ \mathbf{0} & \mathbf{D}_M^{-1} & \mathbf{0} \\ -\mathbf{W}_P^{-T}\mathbf{W}_B^T & -\mathbf{W}_P^{-T}\mathbf{W}_M^T & \mathbf{W}_P^{-T} \end{bmatrix}. \tag{27}$$

According to the indirect electromechanical analogy [15], the capacitance and reluctance matrices are formed from the mass and stiffness matrices of the reduced-order model, respectively, after proper reordering of either these matrices or the transformation matrix.

$$\mathbf{C} = \mathbf{R}^T\widehat{\mathbf{M}}\mathbf{R}, \qquad \mathbf{B} = \mathbf{R}^T\widehat{\mathbf{K}}\mathbf{R}. \tag{28}$$

The matrices being transformed are the submatrices given by Equations (22) and (23). With the current ordering of electrical DOFs, the electromechanical coupling matrix is built from $\widehat{\boldsymbol{\Gamma}}$ (Equation (23)) as

$$\boldsymbol{\Gamma}_{EM} = \left[\mathbf{0}, \mathbf{0}, \widehat{\boldsymbol{\Gamma}}\right]. \tag{29}$$

4.3 Coupling assessment

Since matrix transformations defined in Equation (28) do not alter the generalized eigenvalues (as long as the matrix $\mathbf{R}$ is non-singular), the resonance frequencies of the subnetwork are identical to those of the ROM. It may then be assumed that the mechanical mode $\boldsymbol{\phi}_{m,i}$ and its electrical counterpart $\boldsymbol{\phi}_{e,i}$ are dominant in the response of the system around the resonance frequency of a specific mode $\omega_{sc,i}$

$$\mathbf{x} \approx \boldsymbol{\phi}_{m,i}\eta_{m,i}, \qquad \boldsymbol{\psi} \approx \boldsymbol{\phi}_{e,i}\eta_{e,i}, \tag{30}$$

where $\eta_{m,i}$ and $\eta_{e,i}$ are mechanical and electrical modal coordinates, respectively. If the mechanical modes are mass-normalized,

$$\boldsymbol{\phi}_{m,i}^T\widehat{\mathbf{M}}\boldsymbol{\phi}_{m,i} = 1, \qquad \boldsymbol{\phi}_{m,i}^T\widehat{\mathbf{K}}\boldsymbol{\phi}_{m,i} = \omega_{sc,i}^2, \tag{31}$$

and the electrical modes are capacitance-normalized,

$$\boldsymbol{\phi}_{e,i}^T\mathbf{C}\boldsymbol{\phi}_{e,i} = 1, \qquad \boldsymbol{\phi}_{e,i}^T\mathbf{S}\boldsymbol{\phi}_{e,i} = 2\zeta_{e,i}\omega_{sc,i}, \qquad \boldsymbol{\phi}_{sc,i}^T\mathbf{B}\boldsymbol{\phi}_{e,i} = \omega_{sc,i}^2, \tag{32}$$

then, inserting Equation (30) into Equation (24) and projecting the mechanical (electrical) equation on the mechanical (electrical) mode, the following modal coupled equations are obtained

$$\begin{cases} \ddot{\eta}_{m,i} + \omega_{sc,i}^2\eta_{m,i} + \boldsymbol{\phi}_m^T\boldsymbol{\Gamma}_{EM}\boldsymbol{\phi}_{e,i}\dot{\eta}_{e,i} & = \boldsymbol{\phi}_m^T\mathbf{f} \\ \ddot{\eta}_{e,i} + 2\zeta_{e,i}\omega_{e,i}\dot{\eta}_{e,i} + \omega_{e,i}^2\eta_{e,i} - \boldsymbol{\phi}_{e,i}^T\boldsymbol{\Gamma}_{EM}^T\boldsymbol{\phi}_{m,i}\dot{\eta}_{m,i} & = \mathbf{0} \end{cases}. \tag{33}$$

This system has the same form as that given by Equation (1): the mechanical oscillator has modal mass and stiffness of 1 and ω_{sc}^2, respectively, and the electrical oscillator has modal capacitance, conductance and reluctance of 1, $2\zeta_{e,i}\omega_{e,i}$ and $\omega_{e,i}^2$, respectively. These two systems are coupled by a modal constant $\boldsymbol{\phi}_{e,i}^T\boldsymbol{\Gamma}_{EM}\boldsymbol{\phi}_{m,i}$. An EEMCF is defined by analogy to Equation (2) as

$$\widehat{K}_{c,i}^2 \approx \frac{\left(\boldsymbol{\phi}_{e,i}^T\boldsymbol{\Gamma}_{EM}^T\boldsymbol{\phi}_{m,i}\right)^2}{\omega_{sc,i}^2}. \tag{34}$$

Since the electrical mode shapes are related to the mechanical ones by

$$\boldsymbol{\phi}_{e,i} = \mathbf{R}^{-1}\boldsymbol{\phi}_{m,i}, \tag{35}$$

and, by virtue of Equations (26) and (29),

$$\mathbf{R}^{-T}\boldsymbol{\Gamma}_{EM}^T = \mathbf{W}\widehat{\boldsymbol{\Gamma}}^T, \tag{36}$$

Equation (34) may be rewritten as

$$\widehat{K}_{c,i}^2 \approx \frac{\left(\boldsymbol{\phi}_{m,i}^T\mathbf{W}\widehat{\boldsymbol{\Gamma}}^T\boldsymbol{\phi}_{m,i}\right)^2}{\omega_{sc,i}^2} = \frac{w_{\phi_i}^2\gamma_{\phi_i}^2}{\omega_{sc,i}^2} = w_{\phi_i}^2C_p^{\varepsilon}K_{c,i}^2, \tag{37}$$

where

$$\boldsymbol{\phi}_{m,i}^T\mathbf{W} = w_{\phi_i}, \qquad \widehat{\boldsymbol{\Gamma}}^T\boldsymbol{\phi}_{m,i} = \gamma_{\phi_i}, \qquad K_{c,i}^2 = \frac{\gamma_{\phi_i}^2}{C_p^{\varepsilon}\omega_{sc,i}^2}. \tag{38}$$

$K_{c,i}$ and $\widehat{K}_{c,i}$ are the EEMCFs of mode i without and with electrical subnetwork, respectively. Equation (37) shows that in order to maximize the electromechanical modal coupling, w_{ϕ_i} should have a magnitude as large as possible. This magnitude is nonetheless limited by passivity constraints, as will be shown hereafter.

4.4 Passivity

According to Gannett and Chua [16], the nodal admittance matrix must fulfill the following conditions in order to be the admittance matrix of a passive network (i.e., realizable using passive capacitors, resistors, inductors and ideal transformers):

(i) $\mathbf{Y}(s)$ has no poles in $\{s \in \mathbb{C} | \Re(s) > 0\}$ ($\Re$ denotes the real part operator).

(ii) $\mathbf{Y}(\sigma)$ is a real matrix for $\sigma \in \mathbb{R}^+$.

(iii) $\mathbf{Y}(s) + \mathbf{Y}^H(s)$ is positive semidefinite in $\{s \in \mathbb{C} | \Re(s) > 0\}$ (superscript H denotes Hermitian transposition).

(iv) The network associated to $\mathbf{Y}$ is controllable.

According to Equation (25), $\mathbf{Y}(s)$ has one simple pole at $s = 0$ (for a nonzero reluctance matrix), so Condition (i) is satisfied. Condition (ii) is satisfied since $\mathbf{C}$, $\mathbf{S}$ and $\mathbf{B}$ are real matrices. Condition (iv) is also verified. Now, since $\mathbf{C}$, $\mathbf{S}$ and $\mathbf{B}$ are real symmetric matrices, using Equation (25), the matrix

$$\mathbf{Y}(\sigma + j\omega) + \mathbf{Y}^H(\sigma + j\omega) = 2\sigma\mathbf{C} + 2\mathbf{S} + \frac{2\sigma}{\sigma^2 + \omega^2}\mathbf{B} \tag{39}$$

is positive semidefinite for $\sigma > 0$ and $\omega \in \mathbb{R}$ if $\mathbf{C}$, $\mathbf{S}$ and $\mathbf{B}$ are positive semidefinite themselves, which gives the criteria to satisfy Condition (iii). The matrices $\mathbf{C}$ and $\mathbf{B}$ are guaranteed to be positive semidefinite, because they are obtained from a series of reductions and transformations that do not alter this character originating from $\mathbf{M}$ and $\mathbf{K}$. $\mathbf{S}$ can be chosen so as to respect this condition. Now, one must consider that the piezoelectric transducer is integrated into the subnetwork associated with the matrix $\mathbf{C}$. The subnetwork that is to be connected to the transducer is obtained by removing the contribution of the piezoelectric capacitance from $\mathbf{C}$, yielding another capacitance matrix $\mathbf{C}_N$, which is algebraically expressed as

$$\mathbf{C}_N = \mathbf{C} - C_p^\varepsilon \mathbf{e}_P \mathbf{e}_P^T, \tag{40}$$

where $C_p^\varepsilon = \widehat{\mathbf{K}}_e$ (Equation (23) with a single transducer), and the localization vector $\mathbf{e}_P$ is given by

$$\mathbf{e}_P^T = [\mathbf{0}_B, \mathbf{0}_M, 1]\,. \tag{41}$$

The matrix $\mathbf{C}_N$ ceases to be positive definite when one of its eigenvalues becomes zero, or equivalently when its determinant vanishes. The removal of the piezoelectric element from the subnetwork is represented by a rank-one update of the capacitance matrix in Equation (40). Since the matrix $\mathbf{C}$ is assumed non-singular, Lemma 1.1 from [17] may then be used to compute the updated determinant as

$$\det(\mathbf{C}_N) = \det\left(\mathbf{C} - C_p^\varepsilon \mathbf{e}_P \mathbf{e}_P^T\right) = \left(1 - C_p^\varepsilon \mathbf{e}_P^T \mathbf{C}^{-1} \mathbf{e}_P\right) \det(\mathbf{C})\,, \tag{42}$$

which vanishes if the first factor in the right hand side equals zero. Using Equations (26) and (28),

$$\mathbf{e}_P^T \mathbf{C}^{-1} \mathbf{e}_P = \mathbf{e}_P^T \mathbf{R}^{-1} \widehat{\mathbf{M}}^{-1} \mathbf{R}^{-T} \mathbf{e}_P = \mathbf{W}^T \widehat{\mathbf{M}}^{-1} \mathbf{W}. \tag{43}$$

Inserting Equation (43) into Equation (42) yields a passivity constraint

$$\mathbf{W}^T \widehat{\mathbf{M}}^{-1} \mathbf{W} - \frac{1}{C_p^\varepsilon} \leq 0. \tag{44}$$

Using the spectral expansion of the inverse mass matrix, Equation (44) can be rewritten as

$$\mathbf{W}^T \mathbf{\Phi} \mathbf{\Phi}^T \mathbf{W} = \sum_{i=1}^{N} w_{\phi_i}^2 \leq \frac{1}{C_p^\varepsilon}. \tag{45}$$

Equations (37) and (45) show that passivity constrains the maximum modal electromechanical coupling factor attainable by the network. This sets a practical limitation for the choice of $\mathbf{W}$. Large w_{ϕ_i} may result in a negative determinant of $\mathbf{C}_N$, meaning that it is no longer positive semidefinite and thus that the network cannot be realized with passive components. Going back to Equation (27), it is observed that the scaling matrices $\mathbf{D}_B$ and $\mathbf{D}_M$ play no role in coupling or in passivity of the network. The associated variables are purely electrical, internal to the network and not directly coupled to the structure. They are expected to be of importance when the network has to be realized, but this issue is beyond the scope of the present work. Presently, they are chosen arbitrarily, with the only constraint that matrices $\mathbf{D}_B$ for two matching interfaces must be identical in order to maintain compatibility. For simplicity, they are taken equal to identity matrices.

4.5 Network tuning procedure

A passive subnetwork can now be synthesized by choosing a set of N modal coefficients w_{ϕ_i} respecting the passivity constraint (Equation (45)) and then computing its physical form as

$$\mathbf{W}_\phi^T = [w_{\phi_1}, \cdots, w_{\phi_N}], \qquad \mathbf{W} = \mathbf{\Phi}^{-T}\mathbf{W}_\phi. \tag{46}$$

Matrices $\mathbf{C}$ and $\mathbf{B}$ can then be computed using the transformation matrix given by Equation (27) in Equation (28). The EEMCF can be computed with the modal coefficients w_{ϕ_i} from Equation (37). From the knowledge of this EEMCF, the equivalent capacitance (which is unitary in this case) and the resonance frequency $\omega_{sc,i}$, the resistive elements of the networks can be tuned using e.g. the formula given in Yamada et al [11]

$$\boldsymbol{\phi}_{e,i}^T \mathbf{S} \boldsymbol{\phi}_{e,i} = \sqrt{\frac{3\widehat{K}_{c,i}^2}{2}}\omega_{sc,i} = 2\zeta_{e,i}\omega_{sc,i}. \tag{47}$$

Computing this quantity for all the modes to be controlled, the conductance matrix may then be found by

$$\mathbf{S} = \mathbf{\Phi}_e^{-T} \begin{bmatrix} 2\zeta_{e,1}\omega_{sc,1} & & \\ & \ddots & \\ & & 2\zeta_{e,N}\omega_{sc,N} \end{bmatrix} \mathbf{\Phi}_e^{-1} = \mathbf{R}^T \mathbf{\Phi}^{-T} \begin{bmatrix} 2\zeta_{e,1}\omega_{sc,1} & & \\ & \ddots & \\ & & 2\zeta_{e,N}\omega_{sc,N} \end{bmatrix} \mathbf{\Phi}^{-1}\mathbf{R}. \tag{48}$$

The conductance matrix built this way is thus positive semidefinite.

The procedure can be repeated for each substructure, and the capacitance, conductance and reluctance matrices of the global electrical network can be obtained through standard assembly procedures identical to those used for the mechanical structure.

5 Application to a bladed rail

The proposed approach is illustrated with the example of a monolithic bladed rail made of aluminum. The blades of this structure have a rather complex geometry, requiring the use of finite element modeling. It features qualitatively similar dynamics to those of bladed assemblies. Figure 4(a) shows the model of the bladed rail and Figure 4(b) depicts its breakdown into five identical bladed substructures and two edge substructures to apply the proposed method. Each bladed substructure is endowed with a piezoelectric patch placed near the root of the blade, on the underside of the support. The five patches (PIC 255 - 15 mm $\times$ 10 mm $\times$ 0.5 mm) are visible on the bottom view of the structure in Figure 4(c).

The leftmost and rightmost edges of the rail in Figure 4(a) were clamped. Four finite element models were built: one for each edge substructure retaining the interface DOFs, one for a bladed substructure retaining the two interfaces' DOFs, the patch voltage and twenty CNMs, and one for the full structure, retaining the piezoelectric voltage of each patch, the blades' tip displacement DOFs and fifty CNMs. The edges and bladed substructure models were used to synthesize the electrical network, and the ROM of the full structure was used to assess its performance. The finite element models were built using shell elements in the SAMCEF

software [8], and superelement matrices were exported to MATLAB. Modal damping of 0.01% was added to the model, as can be encountered in bladed assemblies [2].

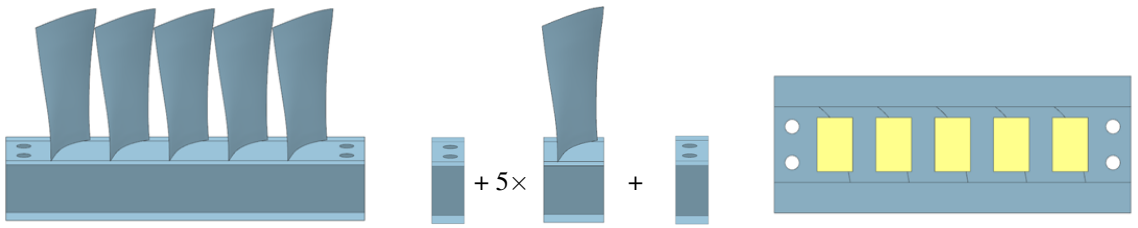

(a) (b) (c)

Figure 4: Bladed rail structure (a), decomposition of the structure (b) and bottom view of the structure featuring the patches (in yellow) (c).

Figure 5 shows the natural frequencies of the bladed rail when the patches are short-circuited. Each frequency given in this work has been normalized with the first resonance frequency. Qualitatively, the modes are organized in two types. The first type is recognizable with the nearly-horizontal lines in the plot. Each line correspond to a family of modes, where the blades vibrate according to one of their cantilever mode shapes. This type of mode is termed blade mode. The modes outside these families features significant motion of the support, and are therefore termed support modes. For illustration, the shapes of the third, eighth, eleventh and fifteenth modes are shown in Figure 6.

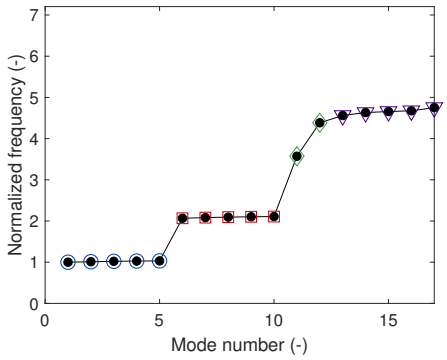

Figure 5: Natural frequencies of the bladed rail with short-circuited patches: family of first blade bending modes (○), family of first blade torsion modes (□), family of second blade bending modes (▽) and support modes (◇).

5.1 Reduced-order model

Figure 7(a) compares the natural frequencies of the full model with those of an assembled model where a various number of CNMs of the bladed substructure are retained (and all the mechanical interface DOFs are used). Figures 7(b) to (d) depict the first three CNMs. Clearly, each CNM is closely related to the cantilever modes of the blade. Including a CNM in the model enables a correct representation of its associated family of modes in the assembled structure.

The influence of the CCMs is now studied, by considering an assembled model with bladed substructures having 20 CNMs, but a variable number of CCMs. Figure 8(a) shows the evolution of the relative error on the natural frequencies for various number of retained CCMs (CCMs with lowest natural frequencies are selected). A relatively good accuracy with less than 2% error is obtained for the blade modes with only one CCM. However, support modes are missing when only one CCM is retained. In general, adding more CCM can reduce the error on the last modes of the blade modes families quite efficiently. A rather large number of CCMs is required to capture the support modes and to increase the accuracy of the first modes of the blade

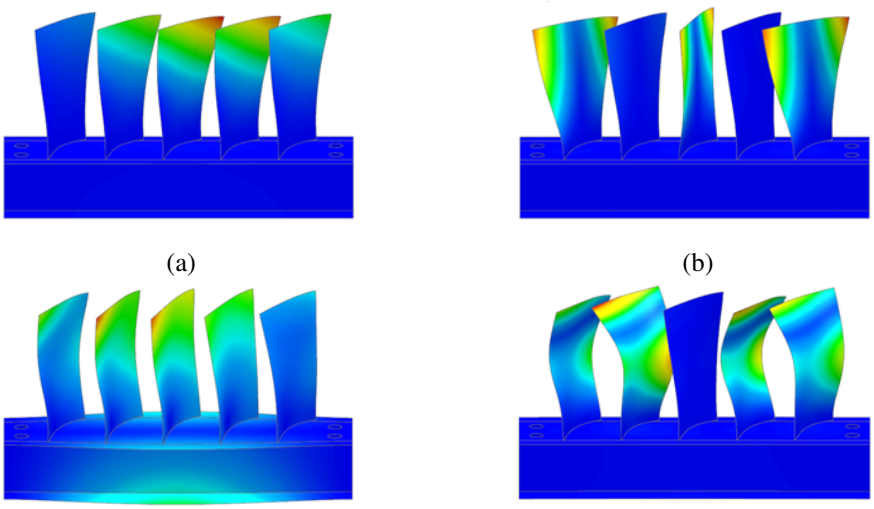

(a) (b) (c) (d)

Figure 6: Mode shapes of the third (a), eighth (b), eleventh (c) and fiftheenth (d) modes of the bladed rail.

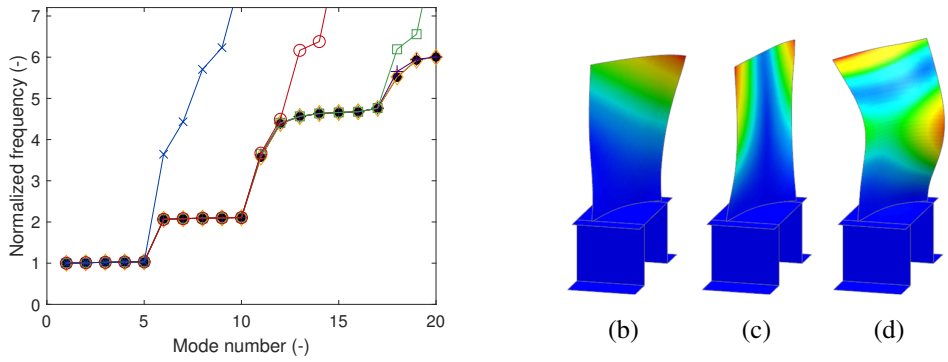

(a) (b) (c) (d)

Figure 7: Natural frequencies of the bladed rail (a) (reference model ($-\bullet-$) and assembled model with 1 ($-\times-$), 2 ($-\circ-$), 3 ($-\square-$), 4 ($-+-$) and 20 ($-\diamond-$) CNMs), first (b), second (c) and third (d) CNM of the bladed substructure (the color scale indicates amplitude of displacement).

modes families. Figure 8(b) shows a more detailed convergence study on specific modes. The fifth mode is the last of the first family of blade modes, and is also the one which involves the least participation from the support. The first mode is still a member of this family, but features more support participation. The eleventh mode is the first support mode. Quite expectedly, modes involving support motion are generally more affected by the CCM truncation.

5.2 Damping performance

An electrical network is now connected to the patches to reduce the vibratory amplitude of the resonant modes at the blades. One CCM is used in the synthesis procedure in regards to the accuracy highlighted previously. At first, a ROM with one CNM and one CCM is synthesized, in order to control the first family of blade modes. The modal coefficients respecting the passivity constraint (Equation (45)) are chosen such that $w_{\phi_1}^2 = 1/C_p^\varepsilon$ and $w_{\phi_2} = w_{\phi_3} = 0$. Emphasis on the first mode is maximized because it corresponds the most to the first cantilever mode of the blade.

The performance of the network is also compared to the performance attainable when the patches are shunted individually with a parallel RL circuit. Each of the five modes of the family is attributed to one patch based

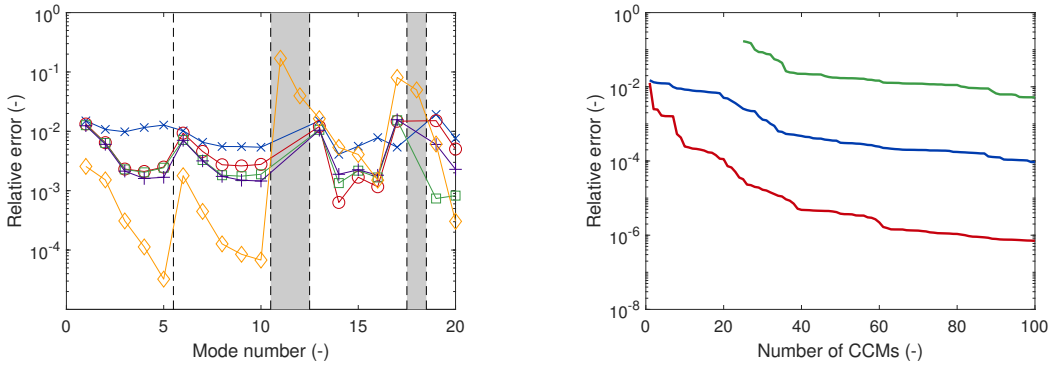

(a) (b)

Figure 8: Relative error on the first twenty natural frequencies of the bladed rail (a) (assembled model with 1 (− × −), 2 (− ○ −), 3 (−□−), 4 (− + −) and 25 (−◇−) CCMs; black dashed lines separate the different families and grey zones indicate support modes) and relative error of the first (—), fifth (—) and eleventh (—) mode as a function of the number of retained CCMs (b).

on the maximization their respective EEMCF. Table 1 details the mode-patch pairs. The resistance and inductance were tuned using Equation (3).

Table 1: Patch number associated to each mode for individual RL shunting.

Mode	1	2	3	4	5
Patch	3	4	5	1	2

Figure 9 shows the FRF of the tip of the fourth blade along its flapwise direction, which is representative of the FRFs of other blades' tip (x_{st}, the static response of the blade under unit force, is used to normalize the amplitude). Appreciable vibration reduction is observed with both techniques, and their performance is somewhat comparable.

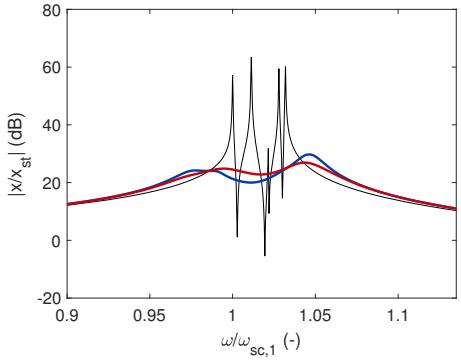

Figure 9: FRF of the fourth blade tip with short-circuited patches (—), with five independent parallel RL shunts (—) and with an electrical network synthesized with one CNM and one CCM (—).

An advantage of the proposed method is that other families can be controlled in a pretty straightforward way. To demonstrate this, a network is synthesized with three CNMs and one CCM, so as to control the three first families of blade modes. Balanced modal coefficients are chosen as $w_{\phi_1}^2 = w_{\phi_2}^2 = w_{\phi_3}^2 = 1/(3C_p^\varepsilon)$ and $w_{\phi_4} = w_{\phi_5} = 0$. Figure 10 shows that the proposed approach is effective to control these three families. The support mode located at $\omega/\omega_{sc,1} = 3.58$ is not damped because it is not captured by the ROM, as discussed earlier. It could be controlled using a rather large number of CCMs, but this would result in a complex network with numerous electrical elements. By contrast, the second support mode located at $\omega/\omega_{sc,1} = 4.38$

is damped, probably because of the control action of the network on the third family, which is quite close in frequency to that support mode.

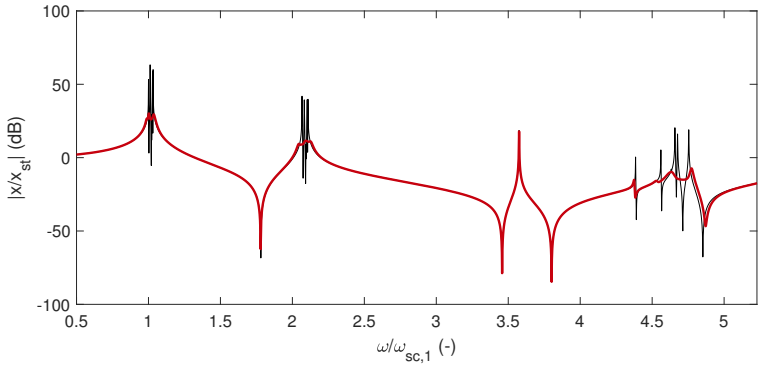

Figure 10: FRF of the fourth blade tip with short-circuited patches (—) and with an electrical network synthesized with three CNMs and one CCM (—).

6 Conclusion

This work proposed to synthesize an electrical network from an assembly of ROMs of substructures in order to provide multimodal vibration mitigation. ROMs were obtained with a classical Craig-Bampton reduction technique followed by a CCM reduction of the interface DOFs. A transformation allowed to obtain matrices describing the network's dynamics from the reduced matrices, and conditions on this transformation to optimize electromechanical coupling while preserving passivity were derived. In particular, it was highlighted that passivity plays the role of a performance limiter. The effectiveness of the proposed approach was illustrated on a bladed rail.

The proposed approach is implementable with standard modeling and numerical techniques, and there is a clear relation between the choices made at design step and the performance of the resulting network. Future works will involve the possibility to include multiple piezoelectric transducers into each substructure. The network realization from passive electrical elements has been left out in this work and shall also be tackled. Finally, the experimental validation of the proposed approach shall be undertaken.

Acknowledgements

The authors would like to acknowledge the financial support of the SPW (WALInnov grant 1610122).

References

[1] N. Hagood and A. von Flotow, "Damping of structural vibrations with piezoelectric materials and passive electrical networks," *Journal of Sound and Vibration*, vol. 146, no. 2, pp. 243–268, apr 1991. [Online]. Available: https://linkinghub.elsevier.com/retrieve/pii/0022460X91907629

[2] B. Mokrani and A. Preumont, "A numerical and experimental investigation on passive piezoelectric shunt damping of mistuned blisks," *Journal of Intelligent Material Systems and Structures*, vol. 29, no. 4, pp. 610–622, 2018. [Online]. Available: https://doi.org/10.1177/1045389X17721023

[3] S. Alessandroni, F. Dell'Isola, and M. Porfiri, "A revival of electric analogs for vibrating mechanical systems aimed to their efficient control by PZT actuators," *International Journal of Solids and Structures*, vol. 39, no. 20, pp. 5295–5324, oct 2002. [Online]. Available: https://linkinghub.elsevier.com/retrieve/pii/S002076830200402X

[4] B. Lossouarn, J.-F. Deü, M. Aucejo, and K. A. Cunefare, "Multimodal vibration damping of a plate by piezoelectric coupling to its analogous electrical network," *Smart Materials and Structures*, vol. 25, no. 11, p. 115042, nov 2016. [Online]. Available: http://stacks.iop.org/0964-1726/25/i=11/a=115042?key=crossref.336b6c7b8578169e34455e93e5f8b4b8

[5] R. Darleux, B. Lossouarn, and J.-F. Deü, "Broadband vibration damping of non-periodic plates by piezoelectric coupling to their electrical analogues," *Smart Materials and Structures*, vol. 29, no. 5, p. 054001, may 2020. [Online]. Available: https://iopscience.iop.org/article/10.1088/1361-665X/ab7948

[6] J. Tang and K. W. Wang, "Vibration Control of Rotationally Periodic Structures Using Passive Piezoelectric Shunt Networks and Active Compensation," *Journal of Vibration and Acoustics*, vol. 121, no. 3, pp. 379–390, jul 1999. [Online]. Available: https://asmedigitalcollection.asme.org/vibrationacoustics/article/121/3/379/441607/Vibration-Control-of-Rotationally-Periodic

[7] J. Liu, L. Li, P. Deng, and C. Li, "A Comparative Study on the Dynamic Characteristics of Bladed Disks With Piezoelectric Network and Piezoelectric Shunt Circuit," in *Volume 7A: Structures and Dynamics*, vol. 7A-2016, no. March. American Society of Mechanical Engineers, jun 2016. [Online]. Available: https://asmedigitalcollection.asme.org/GT/proceedings/GT2016/49835/Seoul,SouthKorea/238633

[8] V. Piefort, "Finite Element Modelling of Piezoelectric Active Structures," Ph.D. dissertation, Université Libre de Bruxelles, 2001. [Online]. Available: https://scmero.ulb.ac.be/Publications/Thesis/Piefort01.pdf

[9] O. Thomas, J.-F. Deü, and J. Ducarne, "Vibrations of an elastic structure with shunted piezoelectric patches: efficient finite element formulation and electromechanical coupling coefficients," *International Journal for Numerical Methods in Engineering*, vol. 80, no. 2, pp. 235–268, oct 2009. [Online]. Available: http://doi.wiley.com/10.1002/nme.2632

[10] I. Giorgio, A. Culla, and D. Del Vescovo, "Multimode vibration control using several piezoelectric transducers shunted with a multiterminal network," *Archive of Applied Mechanics*, vol. 79, no. 9, pp. 859–879, sep 2009. [Online]. Available: http://link.springer.com/10.1007/s00419-008-0258-x

[11] K. Yamada, H. Matsuhisa, H. Utsuno, and K. Sawada, "Optimum tuning of series and parallel LR circuits for passive vibration suppression using piezoelectric elements," *Journal of Sound and Vibration*, vol. 329, no. 24, pp. 5036–5057, nov 2010. [Online]. Available: http://dx.doi.org/10.1016/j.jsv.2010.06.021

[12] R. R. Craig and M. C. C. Bampton, "Coupling of substructures for dynamic analyses." *AIAA Journal*, vol. 6, no. 7, pp. 1313–1319, jul 1968. [Online]. Available: https://arc.aiaa.org/doi/10.2514/3.4741

[13] M. Géradin and D. J. Rixen, *Mechanical vibrations: theory and application to structural dynamics*. John Wiley & Sons, 2014.

[14] M. P. Castanier, Y.-C. Tan, and C. Pierre, "Characteristic Constraint Modes for Component Mode Synthesis," *AIAA Journal*, vol. 39, no. 6, pp. 1182–1187, jun 2001. [Online]. Available: https://arc.aiaa.org/doi/10.2514/2.1433

[15] A. Bloch, "Electromechanical analogies and their use for the analysis of mechanical and electromechanical systems," *Journal of the Institution of Electrical Engineers - Part I: General*, vol. 92, no. 52, pp. 157–169, apr 1945. [Online]. Available: https://digital-library.theiet.org/content/journals/10.1049/ji-1.1945.0039

[16] J. Gannett and L. Chua, "Frequency Domain Passivity Conditions for Linear Time-Invariant Lumped Networks," EECS Department, University of California, Berkeley, Tech. Rep. UCB/ERL M78/21, May 1978. [Online]. Available: https://www2.eecs.berkeley.edu/Pubs/TechRpts/1978/28925.html

[17] J. Ding and A. Zhou, "Eigenvalues of rank-one updated matrices with some applications," *Applied Mathematics Letters*, vol. 20, no. 12, pp. 1223–1226, dec 2007. [Online]. Available: https://linkinghub.elsevier.com/retrieve/pii/S0893965907000614